Solution Properties and Thermal Behavior of Poly(*N*-*n*-propylacrylamide) in Water

Daisuke Ito and Kenji Kubota*

Department of Biological and Chemical Engineering, Faculty of Engineering, Gunma University, Kiryu, Gunma 376, Japan

Received July 8, 1997; Revised Manuscript Received October 9, 1997[⊗]

ABSTRACT: Various molecular parameters characterizing the solution properties of poly(*N*-*n*-propylacrylamide) (PNnPAM) in water were determined over the molecular weight range of (13.3 to 159) × 10^4 at 10 °C by use of light scattering and viscosity measurements. PNnPAM molecules behave as highly hydrated flexible coils. The Laplace inversion method of autocorrelation function of the scattered light intensity ascertained the molecular weight dependence of molecular parameters. Thermal response of PNnPAM molecules in water was studied concerning that the PNnPAM gel exhibits a unique and sharp volume phase transition in contrast to poly(*N*-isopropylacrylamide) gel. Drastic decrease of the second virial coefficient was observed in a very narrow temperature region near the theta temperature, which was determined to be 22.54 ± 0.01 °C. Thermal response of PNnPAM molecules was discussed relating to the excluded volume effect, the hydrophobic interaction, and the chain stiffness.

Introduction

Gels consist of three-dimensional polymer network with cross-linking developed macroscopically. Thermodynamic properties of gel are related to the structure of cross-linking, the interaction between network polymer and solvent, and the interaction between network polymer and network polymer. It has been shown that gels exist in two states, swollen and collapsed phases.[1] The transition between these two phases is termed the volume phase transition and has been an exciting problem for polymer science. Transition is induced reversibly by external conditions: temperature, solvent composition, ionic strength, pH, and so on. Such external conditions change the interaction of network polymer−solvent and polymer−polymer, and those interactions are classified into the van der Waals force, the hydrogen bonding, hydrophobic interaction, and electrostatic interaction.[2] The combination of those four interactions exhibits unique and complex phase behaviors of gel, for example, existence of multiple phases of gels.[3] Therefore, it is very important to examine the characteristic nature of those interactions, and this point can be clarified through the solution properties of molecularly dispersed linear (or branched) polymers.

Aqueous gels have attracted special attention because of the variety of interactions. The most typical one of such gels is poly(*N*-isopropylacrylamide) gel (PNiPAM gel). PNiPAM gel shows discontinuous volume change with temperature change. It has been demonstrated that the volume change results from the coil−globule transition of the PNiPAM chain driven by the hydrophobic interaction. On the other hand, poly(*N*-*n*-propylacrylamide) gel, PNnPAM gel, the homologue of PNiPAM gel, shows very different phase behavior from PNiPAM: lower transition temperature, pronounced swelling ratio at the transition point, and much sharper discontinuous transition.[4] It has been predicted by Tokita et al. previously that PNnPAM molecules should be stiffer than PNiPAM.[5] Solution properties of PNiPAM have been studied well before, and PNiPAM molecules are flexible in water at apart from the transition temperature as much as, e.g., polystyrene.[6] The structure of main chain of PNnPAM is a C−C bond and should not be so stiff intrinsically. Therefore, the difference must result from the side chain *n*-propyl group. Relating to this point, a two-stage coil-to-globule transition observed in polystyrene in cyclohexane should be noteworthy; that is, the crumpled globule is firstly formed and then it shrink to a compact globule.[7] In this mechanism, crumpling may cause the increase of stiffness. Hydrophobic interaction between side chain *n*-propyl groups in PNnPAM molecules will enhance such crumpling and cause a stiffer chain resulting in a sharp discontinuous volume change.

In this paper we present the studies of characterization of PNnPAM in water compared to PNiPAM, the evaluation of molecular weight distribution by use of the Laplace inversion of the correlation functions,[8] and the thermal response of PNnPAM polymer chains. In the study of characterization we focus our attention on the intrinsic characteristics of polymer chains excluding the effect of polydispersity of molecular weight. Thermal behaviors of the chain dimensions are discussed relating to the hydrophobic interaction, the excluded volume effect, and the chain stiffness.

Experimental Section

Materials. PNnPAM was polymerized from *N*-*n*-propylacrylamide in benzene with azobis(isobutyronitrile) as an initiator. The monomer was synthesized from *N*-*n*-propylamines and acryloyl chlorides by a standard method and was used after thorough purification by recrystallization. The details of polymerization method are described elsewhere.[9] The fractionation of PNnPAM samples was carried out following the procedures for PNiPAM,[10] and seven fractions (sample code A to G) were chosen for the present study from the several fractions thus separated. Distilled and deionized water, the resistivity of which was 18.3 MΩ cm, was used as a solvent. Special attention was paid to preparing the sample solutions so that the temperature does not exceed the transition temperature.

Light Scattering. We used a homemade light scattering photometer, and both the homemade digital correlator (240 channels) and ALV-5000/E multiple-tau digital correlator were used for the correlation function measurements.[11] Scattered intensity measurements and the correlation function measurements were carried out simultaneously. A vertically polarized Ar ion laser (Uniphase, 2104-20SL) operated at a wavelength λ_0 of 488.0 nm was used as the incident beam. The output

[⊗] Abstract published in *Advance ACS Abstracts,* November 15, 1997.

S0024-9297(97)01005-X CCC: $14.00

power of the laser beam was controlled at about 10 mW in order to avoid inducing the transition of PNnPAM molecules by the local heating in the sample cell. Vertically polarized scattered light was detected by a photomultiplier tube using the photon-counting method. A cylindrical cell having a 10 mm outer diameter was placed in a thermostated silicon oil bath, the temperature of which was controlled within 0.01 °C. Scattered light intensities at the scattering angle over 25−135° were measured for the static light scattering and the correlation functions measured over 30−60° for the dynamic light scattering.

Optical purification of the sample solutions was achieved by ultracentrifugation and filtration through membrane filters. Both were carried out in a cold room (∼5 °C) in order to avoid the formation of aggregates. The specific refractive index increment, dn/dc, of PNnPAM in water at 10 °C was measured using a homemade Brice-type differential refractometer and was 0.178 cm^3/g.

Viscosity. A Ubbelohde type capillary viscometer was used to obtain the intrinsic viscosity [η]. The flow time of water at 10 °C was about 1500 s. The Huggins plot, the Fuoss-Mead plot, and the Billmeyer plot were combined to determine [η].

Data Analysis

A Zimm plot was employed to obtain the weight averaged molecular weight, M_w, the second virial coefficient, A_2, and the radius of gyration, R_g.

The autocorrelation functions of scattered light intensity, $G^{(2)}(\tau)$, obtained by the homodyne mode were analyzed by the cumulant expansion and CONTIN methods.[12,13] $G^{(2)}(\tau)$ has the following form related to the normalized electric field correlation function, $g^{(1)}(\tau)$

$$G^{(2)}(\tau) = A[1 + \beta|g^{(1)}(\tau)|^2] \quad (1)$$

where A is a baseline and β is a machine constant relating to the coherence of detection. Generally $g^{(1)}(\tau)$ is expressed by the distribution function $G(\Gamma)$ of the decay rate Γ as

$$g^{(1)}(\tau) = \int G(\Gamma) \exp(-\Gamma\tau)\, d\Gamma \quad (2)$$

where $\int G(\Gamma)\, d\Gamma = 1$. That is, $g^{(1)}(\tau)$ is the Laplace transform of $G(\Gamma)$. $g^{(1)}(\tau)$ is expanded by the cumulant expansion

$$g^{(1)}(\tau) = \exp(-\bar{\Gamma}\tau)[1 + (\mu_2/2!)\,\tau^2 - (\mu_3/3!)\tau^3 + ...] \quad (3)$$

where $\bar{\Gamma}$ (average decay rate) and $\mu_2/\bar{\Gamma}^2$ (normalized variance) are related to $G(\Gamma)$ by

$$\bar{\Gamma} = \int \Gamma G(\Gamma)\, d\Gamma \quad (4)$$

$$\mu_2/\bar{\Gamma}^2 = \int [(\Gamma - \bar{\Gamma})^2/\bar{\Gamma}^2] G(\Gamma)\, d\Gamma \quad (5)$$

The third cumulant method was used to retrieve a reliable average decay rate $\bar{\Gamma}$ in this work.

If the fluctuation of the scattered light intensity comes only from the translational diffusion motion of respective polymer chain, decay rate is expressed by a function of concentration C at the limit of zero scattering angle as

$$\bar{\Gamma}/q^2(q{=}0) = D(C) = D_0(1 + k_D C + ...) \quad (6)$$

with q being the momentum transfer vector, $(4\pi n/\lambda_0)$ sin(θ/2), and θ being the scattering angle. D_0 is the translational diffusion coefficient. The hydrodynamic radius R_h is given by the Stokes−Einstein equation, $R_h = k_B T/6\pi\eta_0 D_0$, where k_B is the Boltzmann constant and η_0 is the solvent viscosity. Moreover, $G(\Gamma)$ is related to the molecular weight distribution by

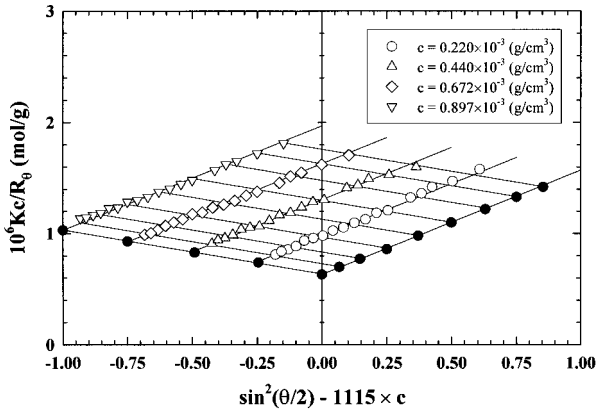

Figure 1. Typical Zimm plot of PNnPAM in water at 10 °C (sample G).

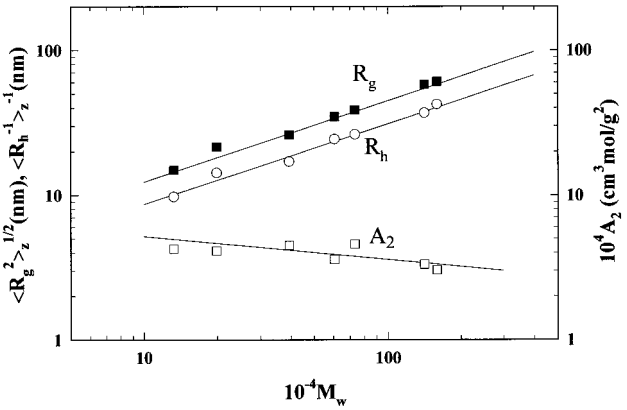

Figure 2. Double-logarithmic plots of the radius of gyration $\langle R_g^2\rangle_z^{1/2}$ (■), hydrodynamic radius $\langle R_h^{-1}\rangle_z^{-1}$ (○), and second virial coefficient A_2 (□) of PNnPAM in water at 10 °C. The solid lines for R_g and R_h denote the molecular weight dependence for monodisperse samples obtained by the analyses of molecular weight distribution. The slopes of the lines for R_g, R_h, and A_2 are 0.56_0, 0.55_6, and −0.16, respectively.

$$G(\Gamma)\, d\Gamma \propto \{W(M)MP(M,q)/[1 + 2A_2W(M)MP(M,q)]\}\, dM \quad (7)$$

where $W(M)$ denotes the weight distribution function of molecular weight, M. The conversion from Γ to M and the evaluation of the scattering function, $P(M,q)$, need the experimental determination of the relationships of R_g and D_0 with M. It should be noted that the experimental molecular weight and squared radius of gyration obtained by Zimm plots are the weight averaged molecular weight M_w and z-averaged squared radius of gyration $\langle R_g^2\rangle_z$, respectively, and the experimental translational diffusion coefficient obtained by correlation function measurements is the z-averaged value $\langle D_0\rangle_z$. Therefore, the relationships of R_g and D_0 (or R_h) with M for the monodisperse case can be obtained by the self-consistent analyses of the molecular weight distribution by the Laplace inversion of the correlation function. This Laplace inversion is known to be an ill-posed problem in nature mathematically,[14] and various methods have been proposed to overcome such an ill-posed problem.[15] The CONTIN 2DP (ALV-CONTIN) method was used in the present work to examine the molecular weight distribution.

Table 1. Characteristic parameters of PNnPAM in water at 10 °C

sample code	$10^{-4}M_w$	10^4A_2 (cm³ mol g⁻²)	$\langle R_g^2\rangle_z^{1/2}$ (nm)	$10^8\langle D_0\rangle_z$ (cm² s⁻¹)	$\langle R_h^{-1}\rangle_z^{-1}$ (nm)	$\langle R_g^2\rangle_z^{1/2}/\langle R_h^{-1}\rangle_z$	$[\eta]$ (cm³ g⁻¹)	k_D (cm³ g⁻¹)	k_f (cm³ g⁻¹)	$k_{D,0}$	$k_{f,0}$	S (nm)	S/R_h	$\mu_2/\bar{\Gamma}^2$	M_w/M_n
A	13.3	4.25	15.0	16.2	9.78	1.53	52.0	25.2	87.1	1.42	4.91	9.1	0.93	0.10	
B	19.9	4.12	21.6	11.1	14.3	1.51		33.8	129	0.91	3.49	11.7	0.82	0.07	
C	39.3	4.49	26.2	9.28	17.1	1.53	101	68.0	284	2.12	8.85	19.0	1.11	0.05	1.10
D	60.6	3.60	35.0	7.85	24.4	1.43		123	313	2.03	5.17	23.6	0.97	0.07	
E	73.3	4.58	38.8	6.03	26.3	1.48	155	159	512	2.54	8.17	29.0	1.10	0.06	1.12
F	141	3.32	58.0	4.17	37.0	1.57	258	177	758	1.95	8.37	40.3	1.09	0.09	
G	159	3.04	60.8	3.74	42.4	1.43	274	192	774	1.59	6.40	42.4	1.00	0.07	

[a] $k_{D,0}$ and $k_{f,0}$ are defined as $k_{D,0} = k_D M_w/N_A V_h$ and $k_{f,0} = k_f M_w/N_A V_h$, respectively, with $V_h = (4\pi/3)R_h^3$. N_A is Avogadro's number. S is the thermodynamic interaction length defined as $(4\pi/3)S^3 = (1/4)A_2M_w^2/N_A$, and S/R_h expresses the reduced interaction length. Variance was the representative value obtained by the third cumulant analyses of correlation functions. M_w/M_n was obtained by CONTIN analysis of correlation function.

Results and Discussion

Characterization of PNnPAM at 10 °C. One of the typical Zimm plots is illustrated in Figure 1. Almost linear behaviors of the inverse scattering functions were obtained for all of the samples. Translational diffusion coefficients and hydrodynamic radii R_h were determined from the correlation functions by using the third cumulant fitting. The numerical data characterizing the solution properties of PNnPAM in water at 10 °C are tabulated in Table 1. The normalized variances, $\mu_2/\bar{\Gamma}^2$, determined from the correlation function measurements are also listed. In the case of relatively narrow molecular weight distribution, $M_z/M_w \sim 1 + 4(\mu_2/\bar{\Gamma}^2)$ holds.[16] Our values of ca. 0.1 of $\mu_2/\bar{\Gamma}^2$ mean that our PNnPAM samples are fairly monodisperse and polydispersity is almost the same as (or less than) PNiPAM samples studied previously. The molecular weight dependence of $\langle R_g^2\rangle_z^{1/2}$, $\langle R_h^{-1}\rangle_z^{-1}$, and A_2 are shown in Figure 2 by a double-logarithmic plot. $\langle R_g^2\rangle_z^{1/2}$ and $\langle R_h^{-1}\rangle_z^{-1}$ are a little larger than those of PNiPAM at 20 °C. Reasonable linear relationships are obtained, and the power law relations hold well for $\langle R_g^2\rangle_z^{1/2}$ and $\langle R_h^{-1}\rangle_z^{-1}$:

$$\langle R_g^2\rangle_z^{1/2} = (1.98 \times 10^{-2})M_w^{0.560}\ (\text{nm}) \quad (8)$$

$$\langle R_h^{-1}\rangle_z^{-1} = (1.44 \times 10^{-2})M_w^{0.556}\ (\text{nm}) \quad (9)$$

A_2 values are positive ($(3-4.5) \times 10^{-4}$ cm³mol/g²) and decrease weakly with the increase of molecular weight, and force fitting gives the exponent of −0.16. The exponents of $\langle R_g^2\rangle_z^{1/2}$ and $\langle R_h^{-1}\rangle_z^{-1}$ are the values between the theta state and the good solvent states. An averaged value of $\langle R_g^2\rangle_z^{1/2}/\langle R_h^{-1}\rangle_z^{-1}$ for all of the samples is about 1.5, typical for the flexible coils in the theta state. These facts indicate that PNnPAM molecules in water at 10 °C behave as flexible coils in a relatively good to intermediate solvent state.

Magnitudes of k_D are larger than those of PNiPAM. From the thermodynamic relation,[17] k_D is expressed by

$$k_D = 2A_2M_w - k_f - \nu \quad (10)$$

where ν is the partial specific volume of the polymer and k_f expresses the concentration dependence of the friction coefficient f as $f = f_0(1 + k_fC + ...)$. k_D represents the dynamic interaction, that is, equilibrium interaction manifested in A_2 plus hydrodynamic interaction manifested in k_f. Therefore, the behavior of k_D is important to study the polymer−polymer interaction. Instead of examining k_D and k_f themselves, the quantities expressed by volume fraction units are more convenient for the study of the hydrodynamic interaction as[18]

$$k_{D,0} = k_D M_w/N_A V_h \quad (11)$$

$$k_{f,0} = k_f M_w/N_A V_h \quad (12)$$

with $V_h = (4\pi/3)R_h^3$ and N_A being Avogadro's number. $k_{D,0}$ and $k_{f,0}$ are then expressed by the interaction length S normalized by the hydrodynamic chain size R_h. S is defined as

$$(4\pi/3)S^3 = A_2M_w^2/4N_A \quad (13)$$

Using S defined above, $k_{D,0} = 8(S/R_h)^3 - k_{f,0}$ neglecting a minor contribution of the partial specific volume of polymer. The relationship of $k_{D,0}$ as a function S/R_h is plotted in Figure 3 together with those of PNiPAM at 20 °C. Various theoretical treatments for the relation of $k_{D,0}$ vs S/R_h have been reported, and the difference between them comes mainly from the model for the polymer−polymer interaction.[19] Two theoretical curves of Yamakawa (solid curve)[20] and Akcasu-Benmouna (dashed curve)[21] are drawn in Figure 3. These two theoretical curves correspond to a Gaussian nondraining limit (low interpenetrating models). Data points locate close to the theoretically predicted curves in accordance with the good (to intermediate) solvent condition, similarly to the case of polystyrene and poly(α-methylstyrene) in good solvents.[22] The agreement with the theoretical predictions is good, suggesting a low interpenetration due to the hydration of PNnPAM molecules. According to Pyun and Fixman,[23] $k_{f,0}$ is a measure of coil interpenetration for flexible chains based on the uniform density sphere model and $k_{f,0}$ is ∼2 for fully interpenetrating coils and is ∼7 for low interpenetration. Our averaged value of $k_{D,0}$ is 1.8, and the averaged value of $k_{f,0}$ is about 6.5 correspondingly, as listed in Table 1. This again means low interpenetration of PNnPAM molecules in water.

Intrinsic viscosity as a function of molecular weight is shown in Figure 4 and Table 1. The power law relation holds well for $[\eta]$ vs M_w similarly to $\langle R_g^2\rangle_z^{1/2}$ and $\langle R_h^{-1}\rangle_z^{-1}$.

$$[\eta] = (1.69 \times 10^{-2})M_w^{0.678} \quad (14)$$

Huggins constants were in the range of 0.3−0.4. It should be noted that the experimental $[\eta]$ is the weight averaged value. Although $A_2M_w/[\eta]$ of flexible coils in good solvents has been observed to be about 1.0−1.2, fairly larger values of 1.7−2.1, except for sample A (1.1), were obtained in the present study.[17] Such large values of $A_2M_w/[\eta]$ have also been obtained for PNiPAM in water.[6] Because the relationship between $k_{D,0}$ and S/R_h agrees with the picture of flexible coils in Gaussian nondraining limit as is shown in Figure 3, these discrepancies may result from large A_2 values and may

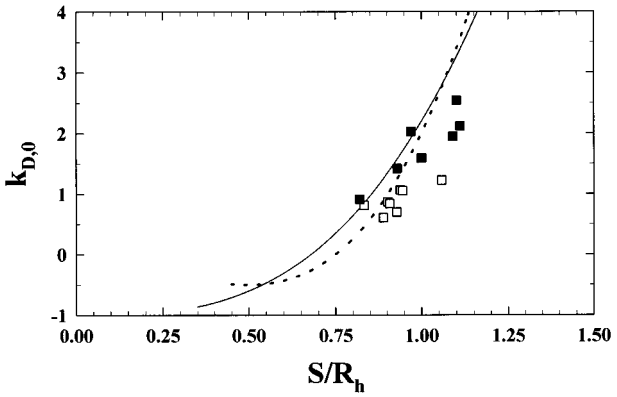

Figure 3. $k_{D,0}$ as a function of S/R_h. ■ stands for PNnPAM at 10 °C, and □ stands for PNiPAM at 20 °C. Solid and dashed curves denote those predicted by Yamakawa theory and Akcasu−Benmouna theory, respectively.

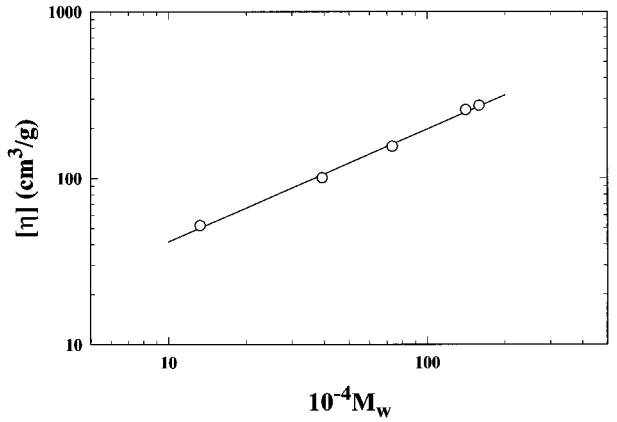

Figure 4. Molecular weight dependence of the intrinsic viscosity $[\eta]$ of PNnPAM in water at 10 °C. The solid line shows the power-law relation of $[\eta] = 1.69 \times 10^{-2}\ M_w^{0.67_8}$. The Huggins constants are in the range of 0.3−0.4.

be correlated with a strong hydration and a unique thermal behavior (excluded volume effect) of PNnPAM molecules.

Molecular Weight Distribution. Laplace inversion analyses were carried out for very dilute solutions of samples C and E. Figure 5 shows the decay rate distribution $G(\Gamma)$ thus obtained. The distribution is fairly narrow corresponding to the results of third cumulant analyses. Molecular weight distribution was calculated according to eq 7 and the resultant distribution functions of samples C and E are illustrated in Figure 6. As noted above, the relations of R_g and D_0 against M for monodisperse case are necessary. Because our samples are fairly monodisperse as suggested by cumulant analyses, it was not so difficult to obtain the self-consistent relations of R_g and D_0 vs M. Indeed those are not much different from eqs 8 and 9, and the exponents should be the same as those of eqs 8 and 9. After several iterations, the relations of

$$R_g = (1.92 \times 10^{-2})M^{0.56_0}\ (\text{nm}) \qquad (15)$$

$$R_h = (1.43 \times 10^{-2})M^{0.55_6}\ (\text{nm}) \qquad (16)$$

give reasonably good results. Weight averaged molecular weight, and z-averaged radius of gyration and translational diffusion coefficient were calculated from the molecular weight distribution function $W(M)$. Those values are listed in Table 2 together with M_z and M_n. The agreements with the experimental results are good

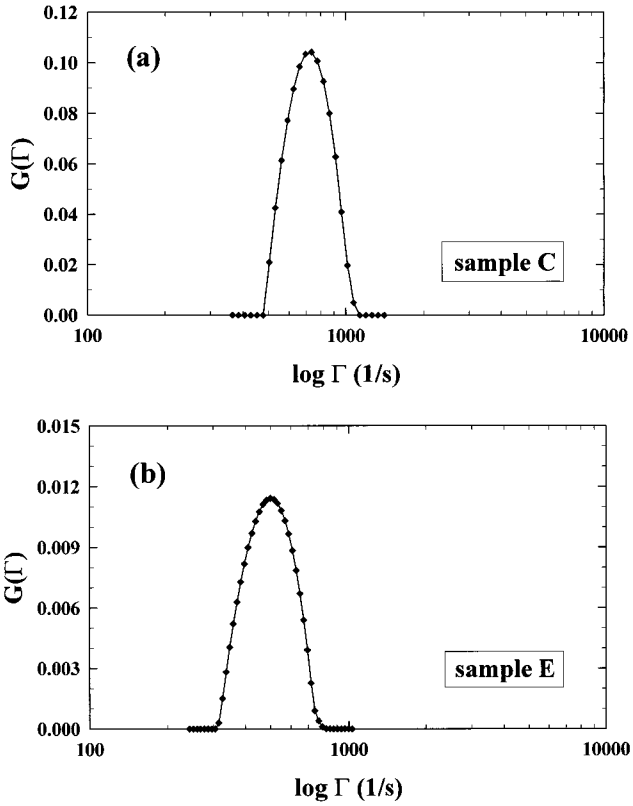

Figure 5. Decay rate distribution $G(\Gamma)$ of PNnPAM obtained by the Laplace inversion of the correlation function: (a) sample C; (b) sample E. Solid curves were drawn to smoothen the data points to guide the eye.

enough. Molecular weight dependences of R_g and R_h were determined excluding the polydispersity effect. Numerical factors in the equations of R_g and R_h increase ca. 3% and 1%, respectively, due to the polydispersity (see eqs 8 and 9). The exponent values of 0.560 and 0.556 of R_g and R_h, respectively, correspond to a good to intermediate solvent condition. The effect of polydispersity for R_h is less than that for R_g as supposed by the Schulz−Zimm distribution function.[24]

Thermal Response and Excluded Volume Effect. Figure 7 shows the temperature dependence of the second virial coefficients of sample G. A_2 decreases with increasing temperature corresponding to LCST-like behavior. This LCST-like temperature dependence is a characteristic of aqueous solution where the hydration and hydrophobic interaction works effectively. A drastically sharp decrease of A_2 was observed near the temperature for $A_2 = 0$. The temperature for $A_2 = 0$, theta temperature, was 22.54 ± 0.01. Temperature dependence of $\langle R_g^2\rangle_z^{1/2}$ and $\langle R_h^{-1}\rangle_z^{-1}$ is shown in Figure 8. $\langle R_g^2\rangle_z^{1/2}$ shows a noticeable decrease in the very narrow temperature range near (lower than) 22.54 °C. Over the temperature 22.56 °C PNnPAM solution becomes very unstable and aggregates easily. These thermal behaviors of PNnPAM molecules are quite different from those of PNiPAM molecules in water. In the case of PNiPAM, $\langle R_g^2\rangle_z^{1/2}$ decreases gradually (very weakly for the sample having the same M_w as the present sample) with the increase of temperature, and PNiPAM molecules are stable over ca. 1 °C above the theta temperature.[25,26]

In order to study this unique thermal behavior of PNnPAM molecules, the relation between A_2 and $\langle R_g^2\rangle_z^{1/2}$ was examined relating to the excluded volume effect. The second virial coefficient is discussed in conjunction

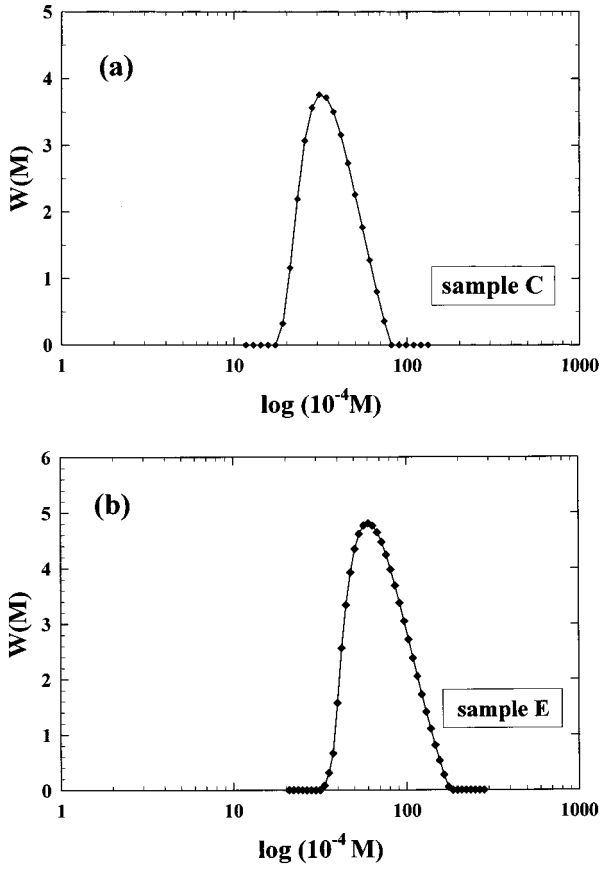

Figure 6. Molecular weight distribution $W(M)$ of PNnPAM: (a) sample C; (b) sample E. $W(M)$ is expressed as the weight fraction in arbitrary units.

with the radius of gyration in terms of the interpenetration function. The interpenetration function, Ψ, is defined by

$$\Psi = A_2 M_w^2/4\pi^{3/2} N_A \langle R_g^2 \rangle_z^{3/2} \quad (17)$$

The interpenetration function expresses the relation of intra- and intermolecular excluded volume effect and is described by the quantities determined experimentally. The recent polymer solution theory based on the two-parameter theory is given by Barrett's theory[27] for Ψ and the Domb−Barrett equation[28] for the expansion factor α_g as

$$\Psi = (z/\alpha_g^3)(1 + 14.3z + 57.3z^2)^{-0.2} \quad (18)$$

$$\alpha_g^2 = [1 + 10z + (70\pi/9 + 10/3)z^2 + 8\pi^{3/2}z^3]^{2/15} \times [0.933 + 0.067 \exp(-0.85z - 1.39z^2)] \quad (19)$$

Here, z is the familiar excluded volume parameter and $\alpha_g = \langle R_g^2 \rangle_z^{1/2}/\langle R_g^2 \rangle_{z,\theta}^{1/2}$ with $\langle R_g^2 \rangle_{z,\theta}^{1/2}$ being the radius of gyration at the theta temperature. $\langle R_g^2 \rangle_{z,\theta}^{1/2}$ was obtained as 49.5 nm from Figure 8. Figure 9 shows the experimental interpenetration function as a function of α_g^3 together with the theoretically predicted curve of TP theory by eqs 18 and 19. In Figure 9, the modified Flory−Krigbaum−Orofino (FKO) theory defined as

$$\Psi = \ln(1 + 5.73z/\alpha_g^3)/5.73 \quad (20)$$

$$\alpha_g^5 - \alpha_g^3 = 1.276z \quad (21)$$

was also drawn for the comparison, because the previous analysis of PNiPAM was carried out using the FKO theory. It should be noteworthy that TP theory of Barrett and Domb−Barrett (eqs 18 and 19) has been recognized to give a better agreement for the excluded volume effect than the FKO theory.[29]

Clear deviation from the TP and FKO theories, especially near $\alpha_g^3 \sim 1$, is observed. It seems that the interpenetration function becomes saturated at $\alpha_g^3 > 1.5$. Although the value ($\Psi \sim 0.25$) at this region is larger than the limiting value (0.24) of TP theory by eqs 18 and 19, the deviation is not unreasonable considering the uncertainty piled up into Ψ. That is, thermal behavior around the plateau region is consistent with a flexible coil indicated by the solution behaviors obtained at 10 °C.

The more critical issue is the systematic deviation at $\alpha_g^3 < 1.5$, and these data points correspond to the region where A_2 and $\langle R_g^2 \rangle_z^{1/2}$ show sharp decrease. Recently, Yamakawa and co-workers proposed quasi-two-parameter theory (QTP theory) of the excluded volume effect based on the helical wormlike chain.[29,30,31] According to their theory, the interpenetration function is not a function of z alone but depends on both the solvent condition (B) and chain stiffness (λ). Here, B expresses the strength of excluded volume dependent upon the local structure of polymer chain. λ is the stiffness parameter and $(2\lambda)^{-1}$ can be approximated to the persistence length.[30] A_2 includes both of the contribution of the chain stiffness and the end (of the chain) effect. Only for sufficiently long chains does the end effect vanish. The chain stiffness modifies both of the intra- and intermolecular excluded volume effects, and the behavior of the interpenetration function reflects the effects of the chain length (molecular weight) and the chain stiffness as well as the solvent condition. In fact, it has been experimentally observed that the interpenetration function against α_g^3 for the variation of the molecular weight exhibits a maximum opposing to the monotonous behavior predicted by the two-parameter theory (atactic- polystyrene[29] and atactic-poly(methyl methacrylate)[38]). The more the stiffness increases, the more the interpenetration function increases more than the TP curve.

This suggests that PNnPAM molecules are fairly stiff at least near the theta temperature. λL is roughly estimated to be <100 from the curves for atactic-polystyrene[29] and atactic-poly(methyl methacrylate)[38] calculated by Yamakawa, where L is the chain contour length. In our case of $M_w = 159 \times 10^4$, contour length can be evaluated to be 3500 nm assuming 0.25 nm for monomer unit length of C−C bonding ($M_L = 452$ nm^{-1}, M_L denotes the molar mass per unit contour length). Then, $(2\lambda)^{-1}$ becomes ca. 18 nm for $\lambda L \sim 100$. This value is too large for the ordinary chemical structure of PNnPAM.

In fact, the combination of $L = 3500$ nm (sample G), d (diameter) = 1.5 nm, and $(2\lambda)^{-1} = 1.2$ nm gives $R_{g,\theta} = 40.4$ nm and $R_{h,\theta} = 25.1$ nm assuming Schulz−Zimm distribution with a distribution parameter of $M_w/M_n = 1.2$. R_g and R_h were calculated using the equations for wormlike chain (KP chain).[32−34] This value of $R_{g,\theta}$ is quite comparable to the value of PNiPAM evaluated before ($\langle R_g^2 \rangle_{z,\theta}/M_w = 10.3 \times 10^{-18}$ cm^2 mol/g for PNnPAM and 9.8×10^{-18} for PNiPAM),[6] and $\lambda B = 0.26$ gives $R_g = 63.9$ nm, $R_h = 39.8$ nm assuming the expansion coefficient of R_h being the same as α_g[35], and $[\eta] = 274$ cm^3/g. These values are in fairly good accordance with the experimental results of sample G at 10 °C. R_g, R_h,

Table 2. Results of CONTIN Analysis of Molecular Weight Distribution of Samples C and E at 10 °C and at the Scattering Angle of 30°

sample C	$10^{-4}M_z$	$10^{-4}M_w$	$10^{-4}M_n$	M_z/M_w	M_w/M_n	$\langle R_g^2\rangle_z^{1/2}$ (nm)	$10^8\langle D_0\rangle_z$ (cm²/s)	$\mu_2/\bar{\Gamma}^2$
CONTIN	41.2	37.3	33.9	1.10	1.10	26.8	9.35	0.03_1
experimental						26.2	9.28	0.05
ratio		0.95				1.02		
sample E	$10^{-4}M_z$	$10^{-4}M_w$	$10^{-4}M_n$	M_z/M_w	M_w/M_n	$\langle R_g^2\rangle_z^{1/2}$ (nm)	$10^8\langle D_0\rangle_z$ (cm²/s)	$\mu_2/\bar{\Gamma}^2$
CONTIN	84.0	74.4	66.3	1.13	1.12	40.0	5.98	0.03_8
experimental		73.3				38.8	6.03	0.06
ratio		1.02				1.03	0.99	

[a] D_0 of the experimental values were determined by the third cumulant analysis. The experimental equatios of $R_g = (1.92 \times 10^{-2})M_w^{0.560}$ and $R_h = (1.43 \times 10^{-2})M_w^{0.556}$ were obtained by the CONTIN analyses.

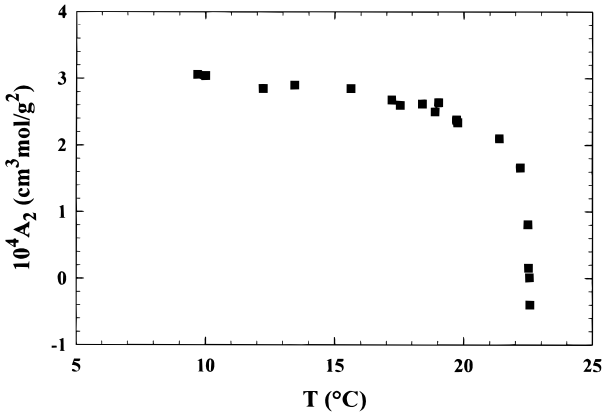

Figure 7. Temperature dependence of the second virial coefficient of sample G ($M_w = 159 \times 10^4$). A drastically steep decrease of A_2 near the theta temperature is clearly observed. The theta temperature was determined to be 22.54 °C.

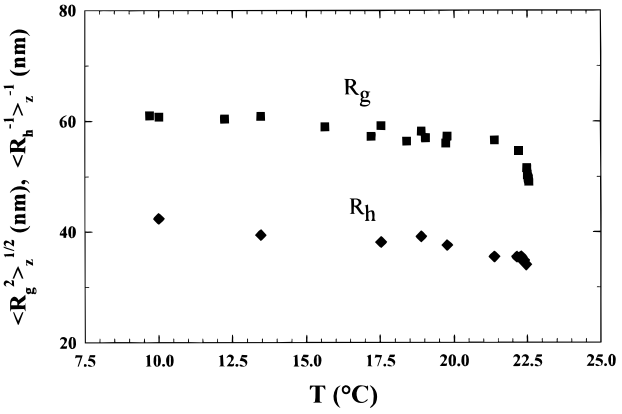

Figure 8. Temperature dependence of $\langle R_g^2\rangle_z^{1/2}$ and $\langle R_h^{-1}\rangle_z^{-1}$ of sample G. At theta temperature $\langle R_g^2\rangle_z^{1/2},_\theta = 49.5$ nm and $\langle R_h^{-1}\rangle_z^{-1},_\theta = 32.4$ nm.

and $[\eta]$, except for $[\eta]$ of samples A and C because of the inapplicability of the Yamakawa−Yoshizaki theory,[34] were evaluated for all other samples using $M_L = 452$ nm^{-1}, $d = 1.5$ nm, $(2\lambda)^{-1} = 1.2$ nm, and $\lambda B = 0.26$, and the calculated values showed the agreement within 10% with the experimental ones at 10 °C. The value of $(2\lambda)^{-1} = 1.2$ nm is quite comparable with typical flexible polymers, e.g., polystyrene.[30] The value of λB seems reasonable considering the good to intermediate solvent condition; for example, $\lambda B \sim 0.4$ was obtained for sodium hyaluronate in aqueous NaCl solution ($(2\lambda)^{-1} \sim 4$ nm).[36] Therefore, QTP theory describes well the behavior at the plateau region, and PNnPAM molecules behave as sufficiently flexible coils with excluded volume effect at ~10 °C.

The discrepancy near the theta point can be elucidated by the idea that PNnPAM chains shrink by local

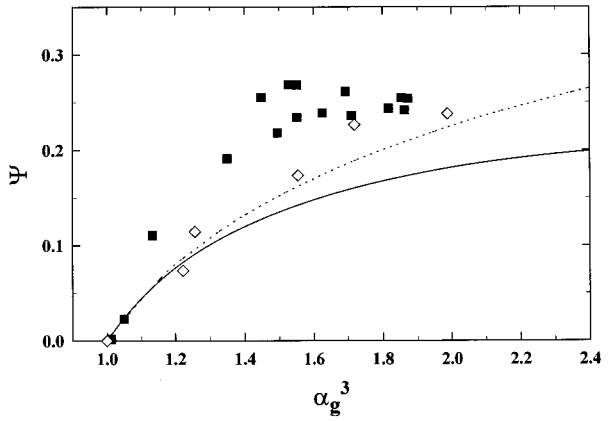

Figure 9. Relationship between the interpenetration function Ψ and the expansion coefficient α_g^3: ■, PNnPAM; ◇, PNiPAM. Solid and dashed curves denote the predicted curves by the TP theory and the FKO theory, respectively.

hydrophobic interaction (for example, lining-up of the *n*-propyl side chains) resulting in the increase of chain stiffness. If $L = 1100$ nm, diameter = 6 nm, and $(2\lambda)^{-1} = 6$ nm are assumed, $R_{g,\theta} = 50.3$ nm, $R_{h,\theta} = 32.0$ nm, and $\lambda L = 92$ are obtained. These values of $R_{g,\theta}$ and $R_{h,\theta}$ agree with the experimental results of $\langle R_g^2\rangle_z^{1/2},_\theta = 49.5$ nm and $\langle R_h^{-1}\rangle_z^{-1},_\theta = 32.4$ nm. $\lambda L = 92$ is consistent with the prediction of the interpenetration function by QTP theory. Of course, there may exist other choices for L and λ, and a definite evaluation of these quantities is difficult at present. However, it is manifest that L must be less and $(2\lambda)^{-1}$ must be larger than those at 10 °C. That is, the PNnPAM chain shrinks, its effective chain diameter becomes enlarged, and the chain becomes stiffer as the temperature approaches the theta temperature. In fact, the ratio $\langle R_g^2\rangle_z^{1/2}/\langle R_h^{-1}\rangle_z^{-1}$, which relates to the segment distribution, shows a slight increase with the increase of temperature. If the chain shrinks with its conformation (stiffness) unchanged, this ratio must decrease contradicting to the experimental observation.

Because the increase of hydrophobic interaction will cause more compact conformation of polymer chain, this physical picture is reasonable enough. The essential role of hydrophobic interaction is ascertained by the fact that the transition temperature increases by about 1 °C in the solution of heavy water, because hydrogen bonding is stronger in heavy water than in ordinary water. A slight systematic deviation of the interpenetration function for PNiPAM is observed as shown in Figure 9, too. It is possible that the same situation as discussed above for PNnPAM might be present in PNiPAM, too. The elongated structure of the *n*-propyl group of PNnPAM is more suitable for a conformational change than the case of the isopropyl group of PNiPAM.

The increase of hydrophobic hydration, structuring of the surrounding water molecules neighboring the *n*-propyl side chain, is agreeable with the large value of molar heat of the transition observed in differential scanning calorimetric measurements.[37] An increase of the chain stiffness results in the enhanced discontinuous volume phase transition of PNnPAM gels.

Conclusion

Various molecular parameters characterizing the solution properties of PNnPAM in water at 10 °C were obtained and the molecular weight dependence of R_g and R_h were ascertained by the molecular weight distribution obtained by the Laplace inversion of correlation function. PNnPAM molecules in water at 10 °C behave as expanded and hydrated flexible coils in a good to intermediate solvent condition. Its conformational structure is almost the same as PNiPAM molecules in water in the stable state.

The temperature dependence of the chain dimension near the theta state shows a unique behavior, and the discrepancy from the conventional excluded volume theory was observed. These phenomena are well explained by the idea that the conformational change of polymer chain in quality occurs approaching the theta temperature: the chain stiffness of PNnPAM molecules increases at close to the theta temperature. This idea explains well the characteristics of the volume phase transition of PNnPAM gel in water.

Acknowledgment. Authors thank Dr. Fujishige of Tokyo Kasei University for providing PNnPAM samples and Dr. M. Tokita of Mie University for his valuable discussion. Authors thank the reviewers for their useful comments, too. This work was supported by a Grant-in-Aid for Scientific Research from the Ministry of Education, Science, and Culture, Japan.

References and Notes

(1) Tanaka, T. *Phys. Rev. Lett.* **1978**, *40*, 820.
(2) Tanaka, T.; Annaka, M.; Ilmain, F.; Ishii, K.; Kokufuta, E.; Suzuki, A.; Tokita. M. *NATO ASI Ser.* **1992**, *H64*, 683.
(3) Annaka, M; Tanaka, T. *Nature* **1992**, *355*, 430.
(4) Inomata, H.; Goto, S.; Saito, S. *Macromolecules* **1990**, *23*, 4887.
(5) Kawasaki, H.; Nakamura, T.; Miyamoto, K.; Tokita, M.; Komai, T. *J. Chem. Phys.* **1995**, *103*, 6241.
(6) Kubota, K.; Fujishige, S.; Ando, I. *Polym. J.* **1990**, *22*, 15.
(7) Chu, B.; Ying, Q.; Grosberg, A. Y. *Macromolecules* **1995,** *28*, 180.
(8) Provencher, S. W. *Comput. Phys. Commun.* **1982**, *27*, 213.
(9) Ito, S.; Fujishige, S. *Kobunshi Ronbunshu* **1989**, *46*, 437.
(10) Fujishige, S. *Polym. J.* **1987**, *19*, 297.
(11) Kubota, K.; Urabe, H.; Tominaga, Y.; Fujime, S. *Macromolecules* **1984**, *17*, 2096.
(12) Koppel, D. E. *J. Chem. Phys.* **1972**, *57*, 4814.
(13) Provencher, S. W. In *Photon Correlation Techniques in Fluid Mechanics*; Schulz-DuBois, E. O., Ed.; Springer: Berlin, 1983.
(14) McWhirter, J. G.; Pike, E. R. *J. Phys. A, Math. Gen.* **1978**, *11*, 1729.
(15) Stepanek, P. In *Dynamic Light Scattering*; Brown, W., Ed.; Clarendon Press: Oxford, 1993.
(16) Pusey, P. N. In *Photon Correlation and Light Beating Spectroscopy*; Cummins, H. Z., Pike, E. R. Eds.; Plenum Press: New York, 1974.
(17) Yamakawa, H. *Modern Theory of Polymer Solution*; Harper & Row: New York, 1971.
(18) Selser, J. In *Light Scattering*; Brown, W., Ed.; Clarendon Press: Oxford, 1996; p 238.
(19) Tsunashima, Y.; Nemoto, N. *Macromolecules* **1984**, *17*, 2931.
(20) Yamakawa, H. *J. Chem. Phys.* **1962**, *36*, 2995.
(21) Akcasu, A. Z.; Benmouna, M. *Macromolecules* **1978**, *11*, 1193.
(22) Han, C. C.; Ackasu, A. Z. *Polymer* **1981**, *22*, 1165.
(23) Pyun, C. W.; Fixman, M. *J. Chem. Phys.* **1964**, *41*, 937.
(24) Zimm, B. H. *J. Chem. Phys.* **1948**, *16*, 1099.
(25) Kubota, K.; Fujishige, S.; Ando, I. *J. Phys. Chem.* **1990**, *94*, 5154.
(26) Wu, C.; Zhou, S. *Macromolecules* **1995**, *28*, 8381.
(27) Barrett, A. J. *Macromolecules* **1985**, *18*, 196.
(28) Domb, C.; Barrett, A. *J. Polym.* **1976**, *17*, 179.
(29) Yamakawa, H.; Abe, F.; Einaga, Y. *Macromolecules* **1993**, *26*, 1898.
(30) Yamakawa, H. *Annu. Rev. Phys. Chem.* **1984**, *35*, 23.
(31) Arai, T.; Sawatari, N.; Yoshizaki, T.; Einaga, Y.; Yamakawa, H.; *Macromolecules* **1996**, *29*, 2309.
(32) Kubota, K; Tominaga, Y.; Fujime, S. *Macromolecules* **1986**, *19*, 1604.
(33) Yamakawa, H.; Fujii, M. *Macromolecules* **1973**, *6*, 407.
(34) Yamakawa, H.; Yoshizaki, T. *Macromolecules* **1980**, *13*, 633.
(35) Douglas, J. F.; Freed, K. F. *Macromolecules* **1985**, *18*, 201.
(36) Hayashi, K.; Tsutsumi, K.; Nakajima, F.; Norisuye, T.; Teramoto, A. *Macromolecules* **1995**, *28*, 3824.
(37) Fujishige, S.; Puttatyaion, S.; Kubota, K.; Ando, I. *Bull. Res. Instit. Polym. Textiles* **1991**, *167*, 39.
(38) Abe, F.; Einaga, Y.; Yamakawa, H. *Macromolecules* **1994**, *27*, 3262.

MA971005S